



Reconfiguration of Bipolar HVDC System for Continuous Transmission Under DC Line Fault

Mitsuyoshi Enomoto , Graduate Student Member, IEEE, Kenichiro Sano , Member, IEEE, Junya Kanno, and Junichi Fukushima

Abstract—This article proposes a reconfiguration method for the bipolar high voltage dc transmission (HVDC) system connecting offshore wind power plants (WPPs). Conventional bipolar HVDC systems can continue to transmit half the rated power even if a dc fault occurs at one of the two poles. However, the shutdown of half of the entire WPPs is inevitable because WPPs cannot continue operations on their own. Once the WPPs are shut down, they take a long time to restart. The power transmission decreases during the time and it imposes a negative effect on the onshore ac system. The proposed reconfiguration method immediately removes the dc fault and relocates the converters and WPPs from the faulted pole to the healthy pole by disconnecting switches. Furthermore, the reconfiguration is designed based on the fault ride-through (FRT) capability of the WPPs specified by the existing grid code. As a result, the reconfiguration realizes the continuous operation of the entire WPPs even if a dc line fault occurs. Therefore, the proposed method can improve the supply reliability. The validity of the proposed method is verified by electromagnetic transient (EMT) simulations.

Index Terms—Bipolar, dc line fault, high voltage dc (HVDC) transmission system, modular multilevel converters (MMC), reconfiguration.

I. INTRODUCTION

WIND power generation is attracting attention as one of the renewable energies [1]. When a wind power plant (WPP) is located offshore, it requires the transmission system for connecting them to an onshore grid. An option is a high-voltage dc transmission (HVDC) system with modular multilevel converters (MMC) [2]. There are three basic configurations in HVDC systems: asymmetric monopolar, symmetrical monopolar, and bipolar configuration [3]. Among them, the bipolar configuration is suitable for improving supply reliability because it can continue to operate one of the two poles even if a dc fault occurs [4]. Some articles focus on the dc fault clearance in bipolar configuration. The fault clearing method using ac

Manuscript received 2 October 2023; revised 27 December 2023 and 22 February 2024; accepted 8 March 2024. Date of publication 25 March 2024; date of current version 16 May 2024. This work was supported in part by the Japan Society for the Promotion of Science (JSPS) under KAKENHI Grant 21K04018, and in part by the Japan Power Academy. Recommended for publication by Associate Editor X. Pei. (Corresponding author: Mitsuyoshi Enomoto.)

Mitsuyoshi Enomoto and Kenichiro Sano are with the Department of Electrical and Electronic Engineering, Tokyo Institute of Technology, Tokyo 152-8552, Japan (e-mail: enomoto.m@peel.ee.e.titech.ac.jp; sano@ee.e.titech.ac.jp).

Junya Kanno and Junichi Fukushima are with the TEPCO Research Institute, Tokyo Electric Power Company Holdings, Yokohama 230-8510, Japan (e-mail: kanno.junya@tepcoco.jp; fukushima.junichi@tepcoco.jp).

Color versions of one or more figures in this article are available at <https://doi.org/10.1109/TPEL.2024.3381218>.

Digital Object Identifier 10.1109/TPEL.2024.3381218

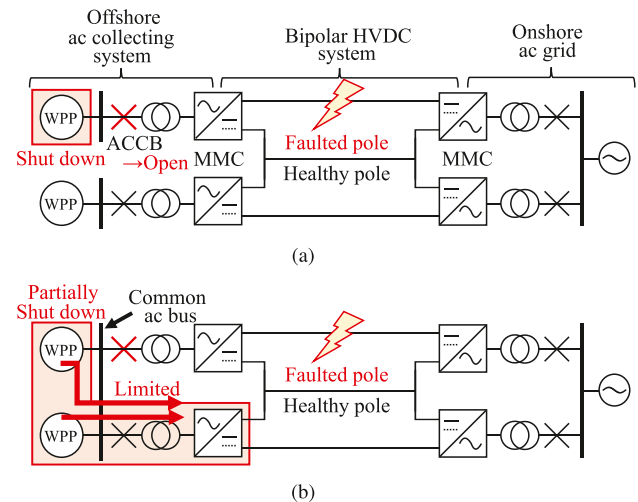


Fig. 1. Connection of WPPs in a bipolar HVDC system. (a) Connecting a single WPP to each pole independently. (b) Connecting WPPs on a common ac bus.

circuit breakers (ACCB) has been put into practical use [5]. Other articles propose the method using enhanced MMCs with fault blocking capability, such as full bridge cells [6], [7], clump double cells [8], and hybrid cells [9], [10]. The use of dc circuit breakers is also an option [11], and dc circuit breakers rated up to 500 kV [12] has been developed. These methods achieve a good performance against dc faults, in particular, the power transmission can be resumed immediately after the deionization time when they are nonpermanent faults. However, these articles focus on the HVDC system as an interconnector between ac grids. Additional investigations are required for applying the bipolar HVDC system for connecting offshore WPPs.

There are two possible configurations of the ac collecting system in the bipolar HVDC system for connecting WPPs as shown in Fig. 1. One, shown in (a), connects a single WPP to each pole independently. The other, shown in (b), connects the WPPs on a common ac bus. In the type (a), the WPP connected to the faulted pole should be shut down when the dc fault is cleared by the method using ACCBs. The offshore ac collecting system is composed of the WPP and the offshore MMC, but it has no synchronous generators [13]. Thus, the offshore MMC forms the grid voltage, and the grid-tied inverters of the WPP control the current in-phase with the grid voltage [14]. Therefore, after the ACCB opens and disconnects the offshore MMC from the offshore ac collecting system, its grid voltage is not determined

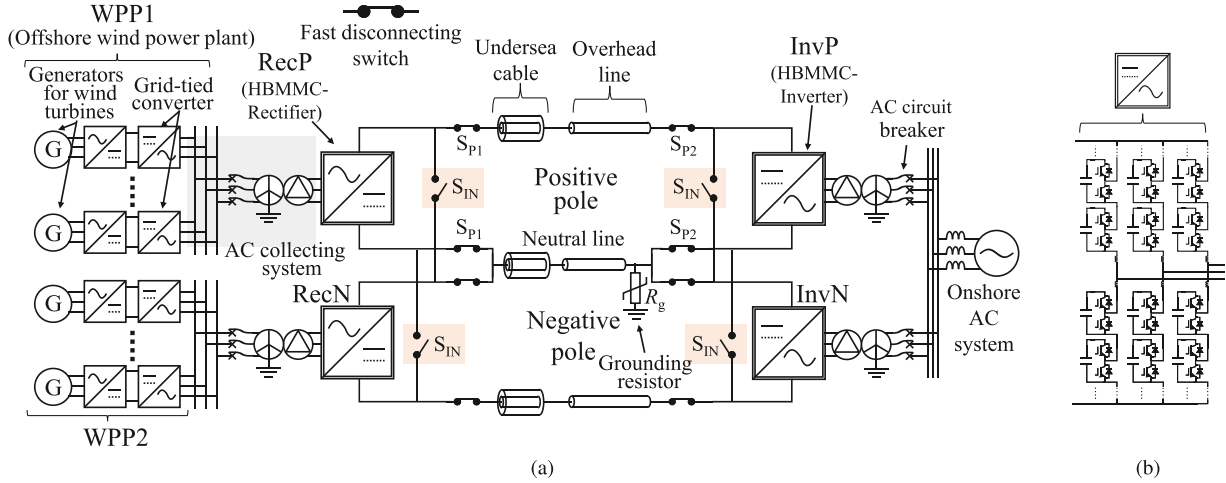


Fig. 2. Configuration of the proposed reconfigurable bipolar HVDC system. (a) Entire system. (b) Half-bridge based MMC (HBMMC).

and the grid-tied inverters cannot continue their operations. This leads to the shutdown of the WPP connected to the faulted pole.

On the other hand, in the type (b), even if the faulted pole is stopped, the MMC on the healthy pole may continue to form the offshore ac grid voltage. Therefore, power transmission can be continued via the healthy pole. However, power flow is limited by the rated power of the MMCs on the healthy pole [15], which is typically half the rated power of the entire bipolar HVDC system. If the WPPs operate around their rated power, a part of the entire WPPs has to be shut down for avoiding the overload of the MMC. This imposes a negative effect on the onshore ac system, and becomes a challenge when operating GW-scale WPP in particular.

To overcome this challenge, this article proposes a reconfiguration method for the MMC-based bipolar HVDC system. The proposed method enables to relocate the converters and WPPs from the faulted pole to the healthy pole while interrupting the fault current on the dc side. Then, it realizes the continuous operation of entire WPPs after dc faults. The idea of relocation has been originally applied to the HVDC system with offshore dc collection system and dc–dc converters [16]. However, the method was not applicable to the HVDC system composed of the ac collection system and half-bridge MMCs, which have already been introduced worldwide [2]. The relocation of the offshore half-bridge MMCs is achieved in a symmetrical monopolar HVDC system [17]. However, the method was not applicable to the bipolar HVDC system. The dc voltage drop of the bipolar system under pole-to-ground faults is more severe than that of the symmetrical monopolar system, which makes it difficult to interrupt the fault current with a half-bridge MMC. In addition, these previous methods did not clarify the relocation of the onshore MMC, which is also indispensable to fully reconfigure the bipolar system. This article expands the applicability of the reconfiguration method to the MMC-based bipolar HVDC system. There are two major progresses from the previous articles [16], [17]. First, this article achieves interruption of the fault current by the half-bridge MMC using an additional grounding resistor or neutral bus switch (NBS). Second, this article clarifies

the relocation of not only the offshore MMC, but also the onshore MMC.

As a result, the proposed method relocates both offshore and onshore converters, enabling to maintain fully rated power transmission. In addition to this, the proposed reconfiguration method is conducted based on the FRT capability of WPPs determined by the existing grid code [18]. Therefore, as long as WPPs comply the existing grid code, the continuous operation of entire WPPs is realized by the proposed method in this article. The validity of the proposed method is confirmed by electromagnetic transient (EMT) simulation.

II. CONFIGURATION OF THE PROPOSED BIPOLAR SYSTEM

Fig. 2(a) shows the proposed reconfigurable bipolar HVDC system. There are two offshore WPPs (WPP1, WPP2) that apply full-converter based configurations. They are composed of multiple generators for wind turbines and the grid-tied converters. The WPP and offshore MMC (RecP, RecN) compose the offshore ac collecting system. In the system, the offshore MMC controls the grid voltage to be constant in amplitude and frequency. The grid-tied converters of WPP control the ac current in-phase with the grid voltage and supply the generated power. The power of the ac collecting system is converted from ac to dc at the offshore MMC, and injected into a dc transmission line. The MMCs are the conventional half-bridge based MMCs as shown in Fig. 2(b). The dc transmission line is bipolar configuration composed of a cable section at the offshore side and an overhead line section at the onshore side. The onshore MMC (InvP, InvN) controls its dc terminal voltage, whereas the offshore MMC (RecP, RecN) controls its dc terminal current. The dc power transmitted to the onshore side is converted from dc to ac by the onshore MMC. The onshore MMC supplies the power to the onshore ac grid by controlling the ac current in-phase with the grid voltage. Due to the operation described above, the power generated on the offshore side is transmitted to the onshore side.

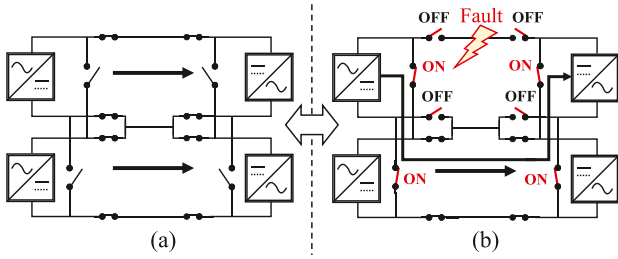


Fig. 3. Possible modes of the proposed system. (a) Point-to-point HVDC mode. (b) Four-terminal HVDC mode.

To realize the reconfiguration, the proposed system is equipped with two types of fast disconnecting switches which operate from 20 to 40 ms. One is the main switch inserted between the dc terminal of the MMC and the transmission line for each of the positive and negative poles. For example, S_{P1} and S_{P2} in Fig. 2(a) are main switches on the positive pole. Similarly, main switches are also inserted on the negative pole. These main switches are closed in the normal operation and connect the MMC and the transmission line at the positive and negative poles, respectively. The other is the interconnection switch S_{IN} inserted between the positive and the negative poles at the dc terminals of the MMCs. The interconnection switches are opened in the normal operation. These two types of fast disconnecting switches operate for the reconfiguration. Furthermore, the system is equipped with some components to support interrupting dc current, such as a grounding resistor R_g with nonlinear characteristic and/or NBS. The NBS, omitted in Fig. 2(a), is described in Section IV-B.

III. RECONFIGURATION WHEN THE FAULT

Fast disconnecting switches enable the proposed system to switch to the following two modes as shown in Fig. 3.

1) The point-to-point HVDC mode: Fig. 3(a)

In the normal operation, the proposed system operates as the point-to-point HVDC system. This is achieved by closing the main switch inserted between the MMC and the transmission line, while opening the interconnection switch inserted between positive and negative poles.

2) The four-terminal HVDC mode: Fig. 3(b)

When a fault occurs, the proposed system changes to the four-terminal HVDC mode. This is achieved by opening the main switch inserted between the MMC and the faulted line, while closing the interconnection switch inserted between positive and negative poles.

“Reconfiguration” in this article refers to the change of the operating mode between the point-to-point HVDC mode and the four-terminal HVDC mode. By the reconfiguration, the power flow interrupted by the fault can be resumed via the healthy pole. For example, when a fault occurs at the positive pole, the power flow on the positive pole is transferred to the negative pole as shown in Fig. 3(b). Since the reconfiguration is performed on the dc side and both of offshore and onshore MMCs are relocated, transmittable power is not limited by the capacity of one MMC. Therefore, there is no need to shutdown the WPP. The proposed reconfiguration is realized through the following three

steps, which are summarized in Fig. 4. Step 1 begins when the fault is detected. Step 2 begins after disconnecting the offshore MMC by turning OFF S_{P1} . Step 3 begins after disconnecting the onshore MMC by turning OFF S_{P2} . Arrows in the diagram indicate the conditions for moving to the next steps. Note that the interconnection switches S_{IN} on the offshore and onshore sides do not have to operate exactly at the same time. Although this article focuses on the fault at the positive pole, the same method can be applied to the fault at the negative pole.

A. Step 1: Suspension of MMCs and Disconnection of the Offshore MMC From the Faulted Pole

When the pole-to-ground fault occurs at the positive pole, the fault current flows through the fault point and the grounding point. When the fault is detected, controller suspends both the offshore MMC (RecP) and the onshore MMC (InvP) with different modes to prevent the discharge of their cell capacitors. The equivalent circuit is shown in Fig. 5, where the negative pole is omitted.

The onshore MMC (InvP) blocks all the switching devices (blocking) as shown in Fig. 6(a). Then, it acts as an uncontrolled diode rectifier and continues to inject the current $i_{F/Inv}$ from the onshore ac system to the dc side as shown in Fig. 5. This current flows through only antiparallel diodes and does not harm insulated gate bipolar transistor (IGBTs). This suspension mode has already been introduced into existing half-bridge MMCs [19].

On the other hand, the offshore MMC (RecP) conducts lower arm short protection [20]. The equivalent circuit during the lower arm short protection is shown in Fig. 6(b). In the cells of the lower arms, high-side IGBT is turned OFF whereas low-side IGBT is turned ON, making a short circuit in the ac side of MMC. The current i_{WPP} flowing from WPP circulates only in the short-circuited lower arms and does not flow out to the dc side as shown in Fig. 5. As mentioned in Section II, WPPs apply full-converter based configurations, where the generators are connected to the offshore MMC via the grid-tied converters. Therefore, i_{WPP} can be controlled by the grid tied converter so that over current does not flow to the short-circuited lower arms of the RecP.

As the dc side is decoupled by the lower arm short protection at the RecP (offshore side), the dc side current $i_{F/Rec}$ decays with time. The decay time can be shortened by inserting current interrupting devices. For example, a nonlinear grounding resistor is inserted as shown in Fig. 5 to interrupt the fault currents $i_{F/Inv}$ and $i_{F/Rec}$.

The circuit equation of $i_{F/Rec}$ becomes as follows:

$$L \frac{d}{dt} i_{F/Rec} = -v_g \quad (1)$$

where L is the total inductance of the transmission line and MMC, and v_g is the voltage across the grounding resistor. The capacitance and resistance of the transmission line are ignored because the grounding resistance is dominant in the current loop. v_g is always positive during this mode because $i_{F/Inv}$ continues to flow. The (1) means that the energy stored in L is dissipated

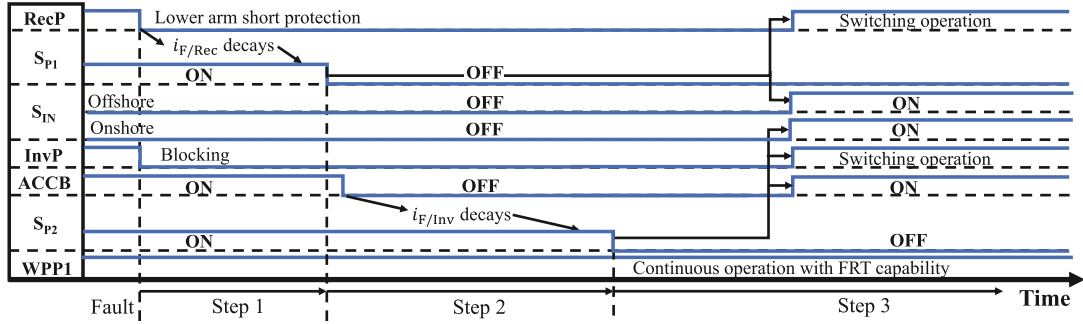


Fig. 4. Time sequence of the proposed reconfiguration with three steps.

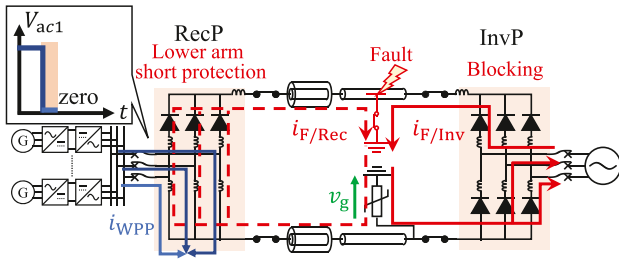


Fig. 5. Step 1: Suspension of MMCs. Offshore MMC conducts lower arm short protection, and onshore MMC conducts blocking.

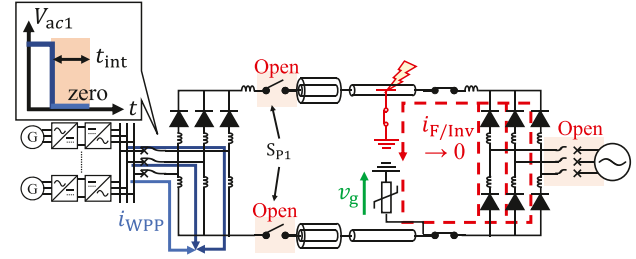


Fig. 7. Step 1 and 2: Disconnection of the offshore MMC from the faulted pole and interruption of the fault current of onshore MMC.

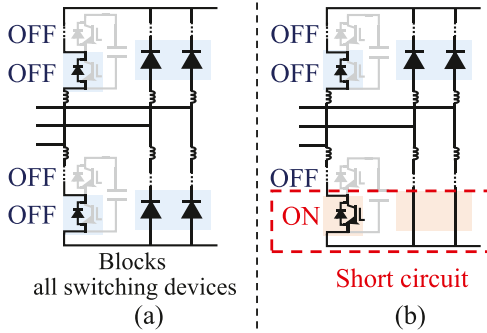


Fig. 6. Detailed states of suspensions for half-bridge MMCs (a) Blocking (Blocks all switching devices), (b) Lower arm short protection.

by the grounding resistor, resulting in the decrease of the fault current $i_{F/Rec}$. When $i_{F/Rec}$ reaches zero, the diodes in upper arms of the RecP are reverse-biased by v_g and hold $i_{F/Rec}$ at zero. After interrupting the fault current $i_{F/Rec}$, the main switches S_{P1} on the offshore side are opened. Then, RecP is disconnected from the faulted pole as shown in Fig. 7. The main switch S_{P1} does not need the fault current interrupting capability because it opens after the current interruption.

B. Step 2: Disconnection of the Onshore MMC From the Faulted Pole

While the operation mentioned above, InvP continues to inject the fault current $i_{F/Inv}$ from the ac side to the dc side. $i_{F/Inv}$ is cleared by opening the ACCB as shown in Fig. 7. When the ACCB is opened, the dc side is decoupled from the ac side.

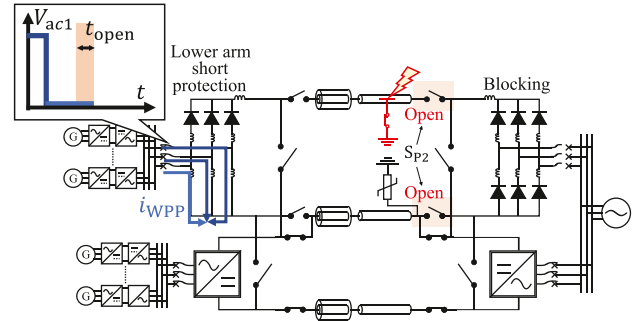


Fig. 8. Step 2: Disconnection of the onshore MMC from the faulted pole.

However, the energy stored in the inductor maintains $i_{F/Inv}$ to flow. The current decays by the grounding resistor, and $i_{F/Inv}$ finally reaches zero. The equation for $i_{F/Inv}$ is expressed in the same way as (1). The decay time can be shortened by inserting the grounding resistor. After the fault current reaches zero, the main switch S_{P2} at the onshore side disconnects InvP from the faulted pole. As a result, both offshore and onshore MMCs are disconnected from the faulted pole as shown in Fig. 8.

During this operation, RecP continues lower arm short protection, resulting in the continuous drop of the ac voltage V_{ac1} on the offshore side as shown in Fig. 8.

C. Step 3: Closing of the Interconnection Switch and the Resumption of the Power Transmission

The interconnection switches S_{IN} and ACCB are closed as shown in Fig. 9, and the disconnected RecP and InvP are

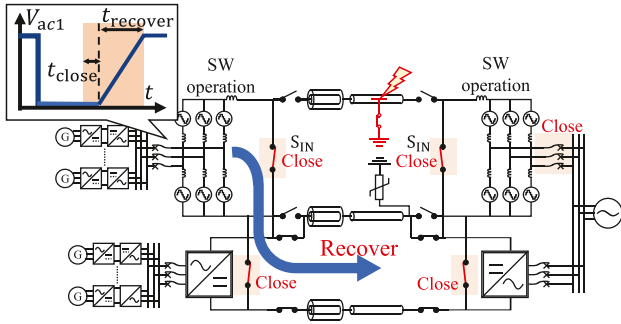


Fig. 9. Step 3: Closing of the interconnection switch and the resumption of the power transmission.

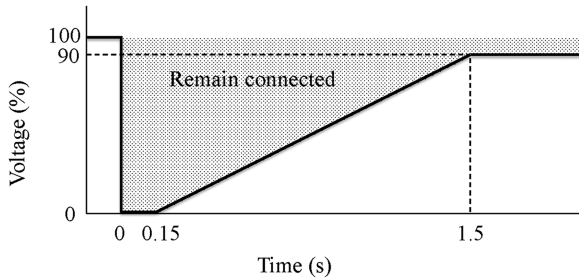


Fig. 10. FRT requirement of the WPP defined by the grid code.

connected in parallel with RecN and InvN, respectively. That is, the system has been reconfigured to the four-terminal HVDC mode. No inrush current flows at this time because RecP and InvP have still been suspended.

Then, both RecP and InvP are deblocked. At this time, InvP and InvN regulating dc side voltage have a $V-I$ drooping characteristic to avoid current imbalance between them. RecP resumes the switching operation and increases the ac voltage V_{ac1} from zero to the rated value as shown in Fig. 9. The voltage recovery restores the power supply from the WPP1 via the ac collecting system and the healthy negative pole as shown in Fig. 9.

IV. DESIGN BASED ON THE FRT REQUIREMENT

A. Requirements for Continuous Operation of the WPPs

The reconfiguration allows to resume the power flow through the healthy pole. On the other hand, it causes a voltage sag at the offshore ac collecting system for WPP1 as shown by V_{ac1} in Fig. 9. This is because RecP makes its ac terminal to be short-circuited for interrupting the fault current. If this voltage sag persists, WPP1 will eventually stop.

The proposed method utilizes the FRT capability of the WPPs. The grid code defines the fault condition under which the WPPs should continue to operate. Therefore, we propose to design the voltage sag during reconfiguration so that the WPP can continue its operation. Fig. 10 shows the specific voltage sag defined in a grid code [18]. There are two periods in the voltage sag. In the zero voltage period, the voltage is allowed to be zero for 150 ms. In the recovery period, the voltage recovers to 90% of the rated

value in 1.5 s. The reconfiguration is designed according to these periods as follows.

The first condition is to satisfy the zero voltage period. t_{int} is the time from the occurrence of the fault to the completion of interrupting the fault current $i_{F/Inv}$. t_{open} is the opening time of the main switch. t_{close} is the closing time of the interconnection switch and the ACCB. When a fault occurs, RecP starts the lower arm short protection. Then, RecP and InvP are disconnected from the faulted pole for the duration of $t_{int} + t_{open}$ (see Figs. 7 and 8). Next, RecP and InvP are connected to the healthy pole for the duration of t_{close} (see Fig. 9). Then, RecP quits the lower arm short protection and resumes the switching operation. The ac voltage V_{ac1} drops to almost zero while RecP conducts the lower arm short protection. Because the zero voltage period should be within 150 ms, the following formula holds to satisfy the FRT requirement.

$$t_{int} + t_{open} + t_{close} = t_{zero} < 150 \text{ ms.} \quad (2)$$

The second condition is to satisfy the recovery period. RecP recovers the ac voltage V_{ac1} from zero to the rated value in a ramp shape for the duration of $t_{recover}$ as shown in Fig. 9. Thus, the following formula should also be satisfied:

$$t_{zero} + t_{recover} < 1.5 \text{ s.} \quad (3)$$

In conclusion, the conditions given by (2) and (3) are the requirements for continuous operation of the WPPs with their FRT capability.

t_{open} and t_{close} are determined by the characteristics of the switches. $t_{recover}$ is determined by the voltage control of RecP. Note that as the converters are at blocking states during the reconfiguration, the control delays of the converters have almost no influence on the satisfaction of (2). Also, regarding (3), the time scale discussed here is much longer compared to the control delay of the converter (approximately less than 100 μ s), and the control delay of the converter has almost no influence on the satisfaction of (3) too. On the other hand, the interruption time t_{int} depends on several factors such as the impedance of the dc system (fault location), the impedance of the ac system, and a fault clearing method.

For example, when the fault location is far from the MMC, the equivalent inductance becomes large, resulting in the increase of the energy stored in the transmission line. This means that the decay time of the fault current becomes longer. In addition, the magnitude of the dc current $i_{F/Inv}$ while the InvP operates as a diode rectifier depends not only on the impedance of the dc side and the MMC, but also on the impedance of the onshore ac system [21]. This means that the energy stored in the inductance changes according to the impedance of the ac system and affects t_{int} .

However, these characteristics are physically determined by the system configuration, such as transmission length and its impedance. Therefore, once the system is characterized, it is possible to adjust t_{int} by designing the fault clearing method properly. For example, if the decay time is relatively long because of the long transmission line, the time can be shortened by increasing the voltage across the grounding resistor v_g in the (1) with increasing its resistance. Equation (2) implies that the

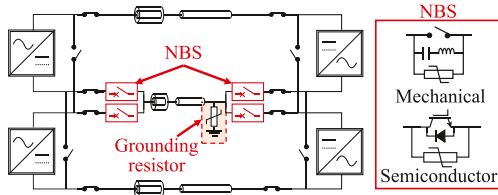


Fig. 11. Optional fault clearing methods to accelerate current interruption.

time required for current interruption (t_{int}) can be extended if the operating time of the disconnecting switches or ac circuit breaker (t_{open} , t_{close}) can be shortened. In order to give more degrees of freedom in design, optional fault clearing methods are described in the following section. Furthermore, the basic design method based on a quantitative analysis is shown in the appendix.

B. Optional Fault Clearing Methods to Accelerate Current Interruption

As mentioned before, the interruption time t_{int} has to be designed to meet the requirement. This section describes optional current interrupting methods to give more degrees of freedom in design.

1) *Grounding Resistor*: The method using a grounding resistor has already been shown in the previous section. The grounding resistor is inserted between the grounding point and the neutral line as shown in Fig. 11. When the pole-to-ground fault occurs, the grounding resistor is inserted in the path through which the fault currents $i_{F/\text{Inv}}$ and $i_{F/\text{Rec}}$ flow and it contributes to decay the fault current. As the grounding resistor is passive element, it is simple and low cost. And the time for interrupting the fault current can be shortened by inserting a large grounding resistance. However, it increases the transient voltage of the neutral line, requiring a higher insulation level. Therefore, there is a limitation in increasing the grounding resistance. If the transmission line is short and its inductance is small, the required voltage across the grounding resistor v_g and the insulation level are relatively low. Thus, this method will be the most reasonable.

2) *NBS*: To accelerate current interruption, the neutral line may be equipped with a NBS [4], [5], [22]. The NBS is inserted between the neutral line and the dc terminal of MMCs as shown in Fig. 11. The NBS operates after the dc side of the MMC is decoupled from the ac side by opening the ACCB [4], [5]. The role of the NBS is to dissipate the energy of the dc side inductance and interrupt residual current immediately. The basic configuration of the NBS is the same as that of a mechanical or semiconductor type dc circuit breakers. However, the NBS does not require operation at the rated transmission voltage because it operates after decoupling the dc side from the ac system. The mechanical type has been put in practical use as the metallic return transfer breaker in the existing bipolar HVDC systems. Moreover, the NBS does not cause the voltage increase of the neutral line because it is not inserted between the grounding point and the neutral line.

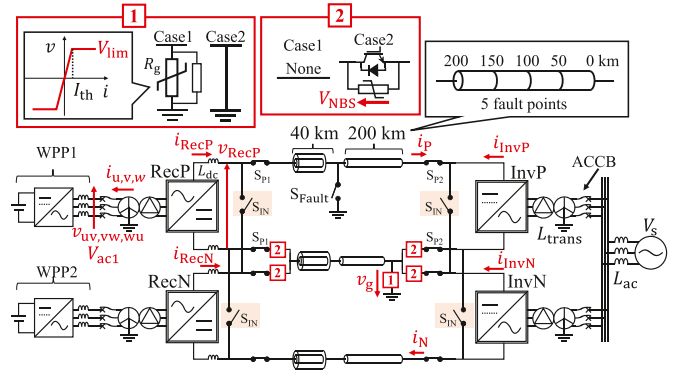


Fig. 12. Simulated system.

If the NBSs are inserted at both the onshore and the offshore sides, the grounding resistor can be removed. The NBS at the onshore side operates after opening the ACCB. This operation is same with [4], [5]. On the other hand, the NBS at the offshore side operates after starting the lower arm short protection of the offshore MMC. The detailed operation is explained at Section VI.

Although the hybrid utilization of a grounding resistor and NBSs may also be an option, the hybrid utilization needs both a grounding resistor and NBSs, which increases components of the system. Therefore, the details are not explained in this article.

V. RECONFIGURATION AFTER FAULT RECOVERY

When the reconfiguration is completed after the fault, all the power from WPP1 and WPP2 flows via the healthy pole. However, continuous operation with this mode can overload the transmission line. Line faults are likely to occur in the overhead line and to be nonpermanent. In such case, the system is reconfigured again from the four-terminal HVDC mode to the point-to-point HVDC mode after the fault arc deionization time of 300 to 500 ms. As a result, the power flow returns to the original state about 1 s after the fault. Thus, transmission lines operate in overload about 1 s. Because the power flow of dc transmission lines is limited only by thermal constraint, dc lines can handle overload for short periods of time. Although it is necessary to design the dc lines taking into account the short-time overload, it is not necessary to double the steady-state current rating.

VI. VERIFICATION BY SIMULATION

The proposed method is verified by EMT simulations using a program XTAP. Fig. 12 shows the simulated system based on Fig. 2. The main differences from Fig. 2 are as follows. The full converter-based WPP is modeled as a set of a dc power supply and a grid-tied inverter. This is because detailed modeling of wind turbine is not necessary as long as verifying the continuous operation capability. The continuous operation of the WPP is confirmed based on the voltage applied to the WPP and FRT requirement. The WPP complying with the FRT requirement is designed to continue its operation under voltage sags that are

TABLE I
CIRCUIT PARAMETERS

Rated power/pole		1000 MVA
Rated dc voltage		± 500 kV
Rated ac voltage	V_s	275 kV
System frequency		50 Hz
Opening time of S_{P1}, S_{P2}	t_{open}	20 ms
Opening time of ACCB		40 ms
Closing time of S_{IN} and ACCB	t_{close}	40 ms
Recover time	$t_{recover}$	100 ms
Clamping voltage of R_g (Case 1)	V_{lim}	100 kV (20%)
Threshold current of R_g (Case 1)	I_{th}	1 A
Clamping voltage of NBS (Case 2)	V_{NBS}	100 kV (20%)
Arm reactance of MMC	L_{arm}	5% (based on 1 pole)
Leakage reactance (onshore)	L_{trans}	15% (based on 1 pole)
AC reactance (onshore)	L_{ac}	20% (based on 2 poles)
DC inductance (offshore)	L_{dc}	60 mH

shorter than the FRT requirement. Therefore, it is possible to assess the continuous operation based on the duration of the voltage sag. Half-bridge MMCs RecP, RecN, InvP, InvN are modeled based on the average value model which can simulate both operating and blocked states. The transmission lines consist of a 40-km cable and four 50-km overhead lines, which are distributed element line models considering frequency-dependent power loss. The distributed element model can simulate the dynamics of an actual cable or overhead line in more detail than the lumped constant model. Pole-to-ground faults are caused in the overhead line by a switch S_{Fault} while both WPP1 and WPP2 generate 1 pu (1 GW). This article focuses on a pole-to-ground fault on an overhead line. This is because the fault occurs more frequently on the overhead line than on the cable. The same method can also be applied even if the fault occurs on the cable. However, in the case of the fault on the cable, the reconfiguration after fault recovery explained in Section V may not be applicable as the fault on the cables may become a permanent fault. The assumed fault points are at 0, 50, 100, 150, and 200 km from InvP.

The parameters are summarized in Table I. They are determined to meet the requirements for continuous operation of WPPs at all the fault points, according to the design procedure in Section IV. Note that the communication delay is supposed to be $5 \mu\text{s}/\text{km}$ [23], assuming the use of optical fiber. Since the total length of the transmission line in the simulation is 240 km, the communication delay between the offshore substation and onshore substation can be calculated as 1.2 ms, and the closing time of the disconnecting switch and ACCB t_{close} is determined including this communication delay. The following waveforms were obtained under the pole-to-ground fault at 200 km from InvP, which took the longest time for the reconfiguration. There are two cases with different fault clearing methods. Case 1 was obtained with a grounding resistor (Only grounding resistor), and case 2 was obtained with four NBSs (Only NBS).

A. Case 1: Fault Clearing With a Grounding Resistor

Fig. 13 shows the simulated result of case 1. The nonlinear characteristics of the grounding resistor are simplified as shown in Fig. 12. The clamping voltage V_{lim} is 100 kV, which is 20% of the rated value, and the threshold current I_{th} is 1 A. In addition,

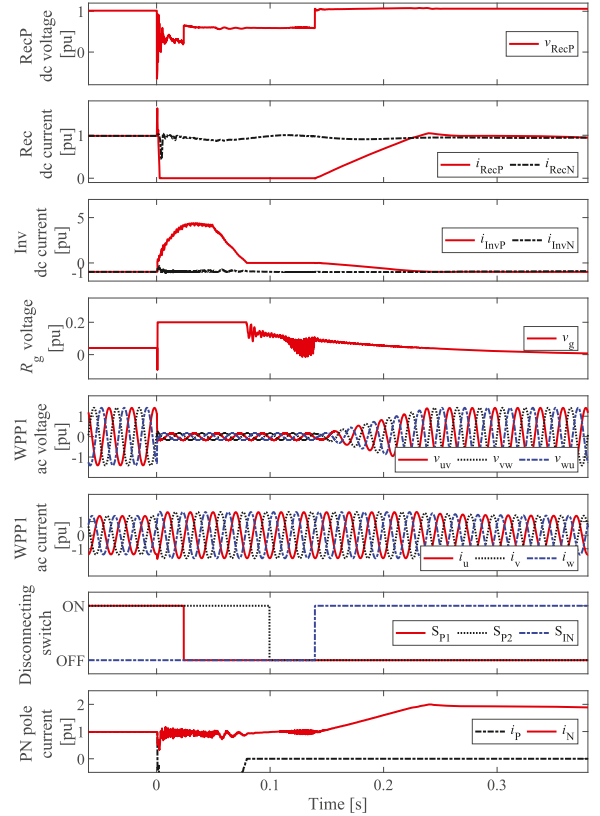


Fig. 13. Simulation waveforms of case 1: A grounding resistor is used for the fault clearing.

a 10-k Ω resistor is inserted in parallel to lower the voltage v_g at steady state. Simulated results are described in the following three procedures.

1) *Step 1: Suspension of MMCs and Disconnection of the Offshore MMC From the Faulted Pole ($0 \text{ ms} \leq t < 24.0 \text{ ms}$):* When the pole-to-ground fault occurred at the positive pole, the voltage of the transmission line v_{RecP} dropped. When this voltage drop was detected, RecP conducted the lower arm short protection. And InvP was blocked due to the increase of the current on dc side. At this time, a trip signal was sent to the ACCB on the onshore side. Due to the lower arm short protection of RecP, voltages of the offshore ac collecting system v_{uv} , v_{vw} , v_{wu} dropped. WPP1 continued to operate while controlling its ac currents i_u , i_v , i_w and generated the residual voltage as shown in v_{uv} , v_{vw} , v_{wu} . These currents flowed in RecP but did not flow to the dc side. As a result, i_{RecP} decreased by the voltage across grounding resistor v_g , which was clamped to 0.2 pu by the grounding resistor. When i_{RecP} reached zero at $t = 4.0 \text{ ms}$, the diodes of the upper arms were reverse biased by v_g and kept i_{RecP} to be zero. Then, a trip signal was sent to the main switches S_{P1} , and they were opened after the operation delay of 20 ms at $t = 24.0 \text{ ms}$. As a result, RecP was disconnected from the faulted pole.

2) *Step 2: Disconnection of the Onshore MMC From the Faulted Pole ($24.0 \text{ ms} \leq t < 99.5 \text{ ms}$):* The blocked InvP acts as an uncontrollable diode rectifier. Thus, the dc current i_{InvP}

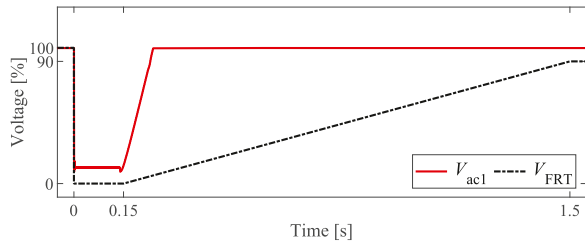


Fig. 14. Comparison with the FRT requirement and the simulation waveform of case 1.

reached five times the rated value. The ACCB beside InvP operated after the operation delay of 40 ms and the dc side was decoupled from the onshore ac side. As a result, i_{InvP} started to decay by the grounding resistor. After i_{InvP} reached almost zero (<0.0025 pu) at $t = 79.5$ ms, the trip signal was sent to the main switches S_{P2} on the onshore side and they were opened at $t = 99.5$ ms after the operating delay of 20 ms. As a result, InvP was disconnected from the faulted pole. During this time, v_{uv} , v_{vw} , v_{wu} had dropped because RecP had continued the lower arm short protection.

3) *Step 3: Closing of the Interconnection Switch and the Resumption of the Power Transmission ($99.5 \text{ ms} \leq t$):* After RecP and InvP were disconnected from the faulted pole, the closing signal was sent to the interconnection switches S_{IN} and the ACCB beside InvP. At $t = 139.5$ ms, the interconnection switches S_{IN} were closed and RecP and InvP were connected to the healthy pole. Then, RecP and InvP resumed the switching operation. RecP gradually restored the ac voltage as shown in v_{uv} , v_{vw} , v_{wu} . As a result, power transmission from WPP1 through RecP was resumed, which was confirmed by the increase of i_{RecP} . No imbalance was observed between i_{InvP} and i_{InvN} because paralleled InvP and InvN controlled their dc voltage with the drooping characteristic. The negative line current i_n has increased to 2 pu, while the positive line current i_p has decreased to 0 pu. This indicates that the power flow was transferred from the faulted positive pole to the healthy negative pole after the reconfiguration. Note that the waveform of i_p during the period $0 \text{ s} < t < 0.09 \text{ s}$ is same as that of i_{InvP} because the InvP is connected to the positive pole at that period.

4) *Validation of Continuous Operation of WPPs:* A voltage sag occurred in the ac collecting system during the reconfiguration. This was confirmed from v_{uv} , v_{vw} , v_{wu} in Fig. 13. The voltage sag has to be small enough to maintain the operation of the WPPs. Fig. 14 shows the comparison with the simulated result V_{ac1} and the FRT requirement V_{FRT} . V_{ac1} is the amplitude of a vector derived by an abc- $\alpha\beta$ transformation of v_{uv} , v_{vw} , v_{wu} . V_{ac1} is above the level of the FRT requirement V_{FRT} , where the WPP continues to operate. Therefore, this voltage sag does not affect the continuous operation of the WPP, as long as the WPP complies with the FRT requirement of the grid code.

Furthermore, Figs. 15 and 16 compare the results with different distances from the fault point. The farther the fault point is from InvP, the longer it takes to interrupt the fault current i_{InvP} . This is because the inductive energy stored in the transmission

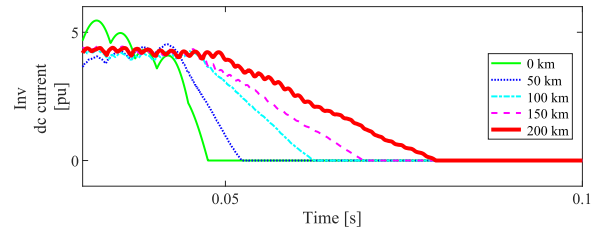


Fig. 15. i_{InvP} obtained under different distances between InvP and the fault point in case 1.

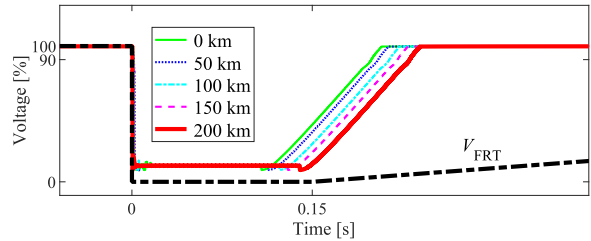


Fig. 16. V_{ac1} obtained under different distances between InvP and the fault point in case 1 and the comparison with the FRT requirement.

line increases as the distance to the fault point. This affects the time required for the reconfiguration as shown in Fig. 16. However, the WPP can continue to operate in all cases because the reconfiguration was designed under the most severe condition, which is the case at the 200-km point. In conclusion, these results verified the successful operation and the design of the proposed reconfiguration.

B. Case 2: Fault Clearing With NBSs

In case 2, four NBSs were applied to clear the fault as shown in Fig. 12. The grounding resistor was removed and the neutral line was directly grounded. The NBS was modeled by an IGBT and a surge arrester whose clamping voltage is 100 kV.

Fig. 17 shows the simulated results of case 2. When the fault occurred, RecP conducted the lower arm short protection and InvP was blocked. Then, NBS of the offshore side operated and interrupted the current i_{RecP} at $t = 2.5$ ms. On the other hand, NBS of the onshore side operated at $t = 46.9$ ms after the ACCB of InvP tripped at $t = 45.9$ ms. As a result, the current i_{InvP} was interrupted at $t = 83.5$ ms. The major differences confirmed from the results are summarized in the following two points.

- 1) The maximum value of i_{InvP} in case 2 is 20% larger compared to case 1. This is because the grounding resistor suppresses the fault current in case 1.
- 2) The neutral line voltage v_g increased to 0.2 pu in case 1, whereas kept at zero in case 2. This is because the system applied the solid grounding in case 2.

Despite these differences, continuous operation of the entire WPP is achieved in both cases. Fig. 18 shows the comparison between the simulated result V_{ac1} and the FRT requirement V_{FRT} . It is confirmed that the voltage sag in case 2 is within the operating range of the FRT requirement. Therefore, the NBSs enabled continuous operation of the entire WPP.

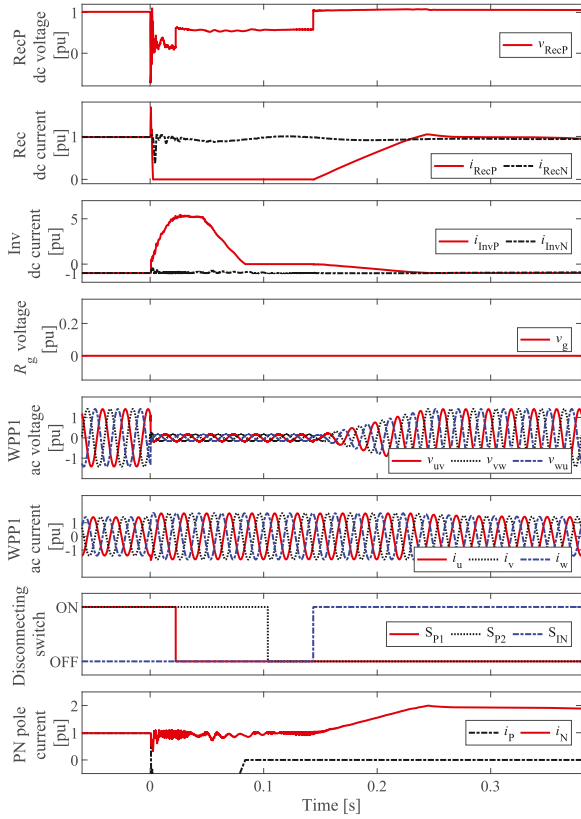


Fig. 17. Simulation waveforms of case 2: NBSs are used for the fault clearing.

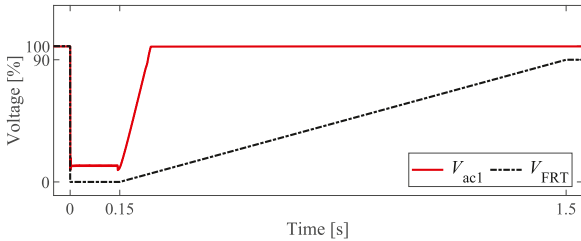


Fig. 18. Comparison with the FRT requirement and the simulation waveform of case 2.

Furthermore, Figs. 19 and 20 compare the results with different distances from the fault point. Fig. 19 shows that the farther the fault point is from InvP, the longer it takes to interrupt the fault current i_{InvP} . This trend is the same as in Fig. 15 when using a grounding resistor. Therefore, same as using the grounding resistor, the WPP can continue to operate in all cases by designing NBSs under the most severe condition (the case where fault occurs at the 200-km point). And it can be confirmed from Fig. 20.

VII. CONCLUSION

This article proposed a reconfiguration method for the bipolar HVDC system. The proposed method realizes continuous operation of the entire WPP even if a pole-to-ground fault occurs. The proposed method utilizes existing MMCs, an ACCB, and

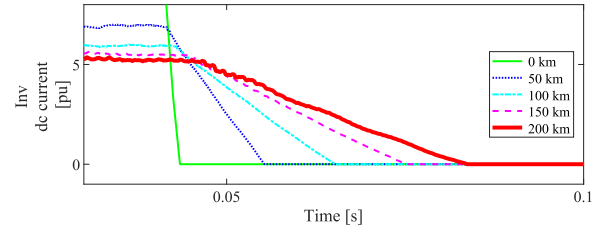


Fig. 19. i_{InvP} obtained under different distances between InvP and the fault point in case 2.

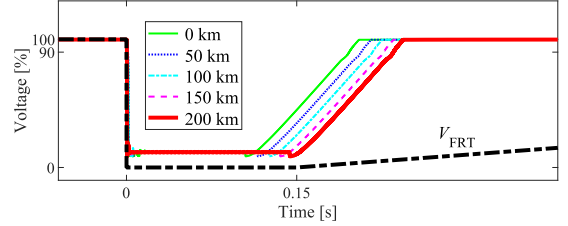


Fig. 20. V_{ac1} obtained under different distances between InvP and the fault point in case 2 and the comparison with the FRT requirement.

a grounding resistor to interrupt the fault current. Additional disconnecting switches enable the HVDC system to reconfigure. The reconfiguration is carried out to meet the FRT requirement of the grid code. The coordination of these components achieved the continuous operation of the WPP complying with the FRT requirement. The proposed method was verified by EMT simulations. The result demonstrated continuous operation of the entire WPP when a pole-to-ground fault occurred.

APPENDIX A

QUANTITATIVE ANALYSIS OF THE CLAMPING VOLTAGE FOR THE GROUNDING RESISTOR AND NBS

This section shows the design procedure of the clamping voltage for the grounding resistor V_{lim} and the NBS V_{NBS} shown in Fig. 12 and Table I. As discussed in Section IV, the reconfiguration must be designed to meet the FRT requirement, and the condition is expressed by (2). For example, the opening time of the main switch is assumed to be $t_{open} = 20$ ms, and the closing time of S_{IN} and ACCB is assumed to be $t_{close} = 40$ ms. Under these conditions, t_{int} must satisfy the following formula.

$$t_{int} < 150 \text{ ms} - (t_{open} + t_{close})$$

$$\therefore t_{int} < 90 \text{ ms.}$$

At the receiving end, t_{int} is the sum of the opening time of the ACCB t_{accb} and the decay time t_{decay} . t_{decay} is defined as the duration from when the ACCB opens until the fault current at the receiving end $i_{F/Inv}$ decays to zero. If t_{accb} is 40 ms, then t_{decay} should satisfy the following formula:

$$t_{decay} < t_{int} - t_{accb}$$

$$\therefore t_{decay} < 50 \text{ ms.} \quad (4)$$

In conclusion, the clamping voltage for a grounding resistor and NBSs should be designed to satisfy the above equation.

TABLE II
 I_{dc} EXPRESSED AS A FUNCTION OF R_{dc} [21]

Mode A	$I_{dc} = \frac{9\sqrt{3}(1-k)U_s}{2\sqrt{(9X_{ac})^2 + (\sqrt{3}(1-k)\pi R_{dc})^2}}$
Mode B	$I_{dc} = \frac{3\sqrt{3}(1-k)\sqrt{3+k^2}U_s}{3X_{ac}(3-k) + \pi R_{dc}(1-k^2)}$
Mode C	$I_{dc} = \frac{3(1-k)k\sqrt{7-4k+k^2}U_s}{k(6-5k+k^2)X_{ac} + \pi R_{dc}(1-k^2)}$
Mode D	$I_{dc} = \frac{3k(1-k)U_s}{k(2-k)X_{ac} + (1-k)\pi R_{dc}}$

TABLE III
BOUNDARY VALUE EXPRESSED BY R_{dc} [21]

Mode A/B	$R_{A/B} = \frac{X_{ac}}{\pi} \frac{9(1+k)}{(3-4k+k^2)}$
Mode B/C	$R_{B/C} = \frac{X_{ac}}{\pi} \frac{(k^2-3k)((k-2)\sqrt{9+3k^2} + 3\sqrt{7-4k+k^2})}{(k^2-1)(\sqrt{9+3k^2} - k\sqrt{7-4k+k^2})}$
Mode C/D	$R_{C/D} = \frac{X_{ac}}{\pi} \frac{(2k-k^2)(\sqrt{7-4k+k^2} - 3+k)}{(k-1)(\sqrt{7-4k+k^2} - 1-k)}$

Then, based on (1), t_{decay} can be calculated from the following equation, where the capacitance and resistance of the transmission line are ignored.

$$t_{decay} \simeq \frac{L}{V_{operate}} I_{dc} \quad (5)$$

where L is the total inductance of the transmission line and MMC, and $V_{operate}$ is the clamping voltage of the grounding resistor or the NBS. I_{dc} is the fault current at the moment of the ACCB operation. I_{dc} is the dc component of the fault current in steady state. In the case of the NBS, the operating time of the NBS t_{NBS} should also be included as follows:

$$t_{decay} \simeq \frac{L}{V_{operate}} I_{dc} + t_{NBS}. \quad (6)$$

Assuming that a fault occurs at the farthest point from the onshore inverter, L becomes maximum and is mainly influenced by the inductance of the transmission line. Therefore, ignoring the inductance of the onshore MMC, L can be approximated by the inductance of the transmission line. In the simulation condition, the inductance and total length of the overhead line are 0.00219 mH/m (@ 1 Hz) and 200 km. Therefore, the total inductance L becomes 438 mH.

Next, I_{dc} can be calculated according to [21]. There are modes A to D as the main steady-state operations of the blocked MMCs when the dc fault. The number of conducting diodes increases from mode A to mode D. In mode A, three diodes conduct continuously. In modes B, C, and D, three and four, four and five, and five and six diodes sequentially conduct, respectively. Note that the intermediate mode is not considered here. The fault current at the dc side in each mode is quoted in Table II. And Table III shows the boundary values expressed by R_{dc} . R_{dc} is the total resistance of the dc side, and U_s is the amplitude of phase voltage of the ac grid. X_{ac} is the reactance of the transformer and the AC grid. The resistance of the ac side is not considered. k is defined as $k = \frac{X_{arm}}{X_{ac} + X_{arm}}$, where X_{arm} is the reactance of the arm reactor.

Tables IV and V are derived by substituting the relation of $V_{dc} = R_{dc}I_{dc}$ into Tables II and III. These formulas are

TABLE IV
 I_{dc} EXPRESSED AS A FUNCTION OF V_{dc}

Mode A	$I_{dc} = \frac{\sqrt{3}(1-k)\sqrt{(9U_s)^2 - (2\pi V_{dc})^2}}{18X_{ac}}$
Mode B	$I_{dc} = (1-k) \frac{3\sqrt{3}\sqrt{3+k^2}U_s - \pi V_{dc}(1+k)}{3X_{ac}(3-k)}$
Mode C	$I_{dc} = (1-k) \frac{3k\sqrt{7-4k+k^2}U_s - (1+k)\pi V_{dc}}{k(6-5k+k^2)X_{ac}}$
Mode D	$I_{dc} = (1-k) \frac{3kU_s - \pi V_{dc}}{k(2-k)X_{ac}}$

TABLE V
BOUNDARY VALUE EXPRESSED BY V_{dc}

Mode A/B	$V_{A/B} = U_s \frac{9\sqrt{3}(1+k)}{4\pi\sqrt{k^2+3}}$
Mode B/C	$V_{B/C} = U_s \frac{3\sqrt{3}k(\sqrt{3(7-4k+k^2)} - (2-k)\sqrt{3+k^2})}{\pi(1+k)(k^2-2k+3)}$
Mode C/D	$V_{C/D} = 3kU_s \frac{(3-k-\sqrt{7-4k+k^2})}{2\pi(1-k)}$

expressed by the voltage of the dc side V_{dc} , and are useful for designing the grounding resistor.

I_{dc} can be calculated using these formulas as follows. Note that the influence of the healthy pole is not considered.

A. Grounding Resistor

In the case of the grounding resistor, it is inserted into the fault current loop before the ACCB operates, which affects I_{dc} . Therefore, this effect should be taken into consideration. By using a grounding resistor, the dc side voltage V_{dc} is almost equal to the clamping voltage of the grounding resistor $V_{operate}$, and the formula in Tables IV and V can be utilized.

First, the specific boundary values for V_{dc} can be obtained by using formulas in Table V and the parameters in Table I as follows:

$$V_{A/B} = 186.8 \text{ kV}, V_{B/C} = 23.2 \text{ kV}, V_{C/D} = 6.7 \text{ kV}.$$

For example, the clamping voltage of the grounding resistor used in the simulation is 100 kV. Since it is smaller than the boundary value between A and B (186.8 kV) and larger than the boundary value between B and C (23.2 kV), it can be seen that the operation is in Mode B. Next, according to the equation for Mode B in Table IV and the parameters in Table I, I_{dc} can be calculated as 8.63 kA, which corresponds to 4.32 pu. This analytical result agrees well with the simulation result of the 200 km line shown in Fig. 15.

The aforementioned process gives us the total inductance L and the fault current I_{dc} . $V_{operate}$ is the operating voltage of the grounding resistor. Substituting them into (5), t_{decay} is calculated to be 37.8 ms, which satisfies (4). A similar decay time was observed in the simulation results for the 200 km line in Fig. 15. This suggests that the clamping voltage of the grounding resistor can be determined theoretically.

B. NBS

In the case of NBSs, the grounding resistor is not inserted on the dc side. Thus, the calculation procedure of I_{dc} is different from that for the grounding resistor. However, in this case, I_{dc} can be calculated using the same method as [21].

The boundary value for R_{dc} can be obtained using the formulas in Table III and the parameters in Table I as follows:

$$R_{A/B} = 26.8 \Omega, R_{B/C} = 2.30 \Omega, R_{C/D} = 0.51 \Omega.$$

Since the grounding resistor is not inserted at the dc side, the resistance of the transmission line is considered as R_{dc} . Ignoring the resistance of the onshore MMC, the total resistance can be obtained by calculating the resistance of the transmission line. The resistance and total length of the overhead line are 0.0101 m Ω /m (@ 1 Hz) and 200 km. Therefore, the total resistance R_{dc} becomes 2.02 Ω . Since it is smaller than the boundary value between B and C (2.30 Ω) and larger than the boundary value between C and D (0.51 Ω), it can be seen that the operation is in Mode C. Then, according to the equation for Mode C in Table II and the parameters in Table I, I_{dc} can be calculated as 10.5 kA, which corresponds to 5.25 pu. This analytical result agrees well with the simulation result of the 200 km line shown in Fig. 19.

The aforementioned process gives us the total inductance L and the fault current I_{dc} , and t_{NBS} is 1 ms in the simulation. Substituting these values and (4) into (6), the lower limit of the clamping voltage $V_{operate}$ can be found as follows:

$$V_{operate} > 93.9 \text{ kV}. \quad (7)$$

The clamping voltage of the NBS is designed to be 100 kV in this article, which satisfies this lower limit. Because the clamping voltage is designed slightly larger than the lower limit, t_{decay} is calculated as 47.0 ms. A similar decay time was observed in the simulation results for the 200 km line in Fig. 19. This suggests that the clamping voltage of the NBS can be designed by the calculation. In practice, resistances of the transmission line and MMC, which are neglected in the equation, also contribute to decay.

In conclusion, it is possible to theoretically obtain the clamping voltage of the grounding resistor and the NBS. Since the aforementioned calculations incorporate approximations, the authors still think that the final design should be validated and tuned through EMT simulation. However, the calculation aforementioned roughly provides us with a suitable design point in advance. Therefore, we can save time by reducing trial and error in the simulation. In addition, parameters related to the design of the grounding resistor and the NBS can be organized.

REFERENCES

- [1] F. Blaabjerg and K. Ma, "Wind energy systems," *Proc. IEEE*, vol. 105, no. 11, pp. 2116–2131, Nov. 2017.
- [2] M. A. Perez, S. Ceballos, G. Konstantinou, J. Pou, and R. P. Aguilera, "Modular multilevel converters: Recent achievements and challenges," *IEEE Open J. Ind. Electron. Soc.*, vol. 2, pp. 224–239, Feb. 2021.
- [3] W. Leterme, P. Tielens, S. De Boeck, and D. Van Hertem, "Overview of grounding and configuration options for meshed HVDC grids," *IEEE Trans. Power Del.*, vol. 29, no. 6, pp. 2467–2475, Dec. 2014.
- [4] A. Hassanpoor, Y.-J. Häfner, A. Nami, and K. Vinothkumar, "Cost-effective solutions for handling DC faults in VSC HVDC transmission," in *Proc. 18th Eur. Conf. Power Electron. Appl.*, 2016, pp. 1–7.
- [5] O. Vestergaard and P. Lundberg, "Maritime link the first bipolar VSC HVDC with overhead line," in *Proc. AEITHVDC Int. Conf. (AEITHVDC)*, 2019, pp. 1–4.

- [6] S. Wenig, M. Goertz, M. Suriyah, and T. Leibfried, "Active DC fault management of a bipolar full-bridge MMC-HVDC scheme with metallic return," in *Proc. IEEE Int. Energy Conf. (ENERGYCON)*, 2016, pp. 1–6.
- [7] S. Wenig, M. Goertz, C. Hirsching, M. Suriyah, and T. Leibfried, "On full-bridge bipolar MMC-HVDC control and protection for transient fault and interaction studies," *IEEE Trans. Power Del.*, vol. 33, no. 6, pp. 2864–2873, Dec. 2018.
- [8] Y. Xue and Z. Xu, "On the bipolar MMC-HVDC topology suitable for bulk power overhead line transmission: Configuration, control, and DC fault analysis," *IEEE Trans. Power Del.*, vol. 29, no. 6, pp. 2420–2429, Dec. 2014.
- [9] X. Yu, Y. Wei, Q. Jiang, X. Xie, Y. Liu, and K. Wang, "A novel hybrid-arm bipolar MMC topology with DC fault ride-through capability," *IEEE Trans. Power Del.*, vol. 32, no. 3, pp. 1404–1413, Jun. 2017.
- [10] T. Wang, G. Song, and K. S. T. Hussain, "Adaptive single-pole auto-reclosing scheme for hybrid MMC-HVDC systems," *IEEE Trans. Power Del.*, vol. 34, no. 6, pp. 2194–2203, Dec. 2019.
- [11] G. Song, T. Wang, and K. S. T. Hussain, "DC line fault identification based on pulse injection from hybrid HVDC breaker," *IEEE Trans. Power Del.*, vol. 34, no. 1, pp. 271–280, Feb. 2019.
- [12] H. Pang and X. Wei, "Research on key technology and equipment for zhangbei 500 kV DC grid," in *Proc. Int. Power Electron. Conf.*, 2018, pp. 2343–2351.
- [13] Z. Li, Y. He, Y. -Z. Li, W. Gu, Y. Tang, and X. -P. Zhang, "Hybrid control strategy for AC voltage stabilization in bipolar VSC-MTDC," *IEEE Trans. Power Syst.*, vol. 34, no. 1, pp. 129–139, Jan. 2019.
- [14] Working Group B4.55, "HVDC connection of offshore wind power plants," CIGRE, Brochure, Tech. Rep. 619, May 2015.
- [15] S. Jiang, Y. Xin, G. Li, and L. Wang, "A novel DC fault ride-through method for wind farms connected to the grid through bipolar MMC-HVDC transmission," *IEEE Trans. Power Del.*, vol. 35, no. 6, pp. 2937–2950, Dec. 2020.
- [16] F. Deng and Z. Chen, "Operation and control of a DC-Grid offshore wind farm under DC transmission system faults," *IEEE Trans. Power Del.*, vol. 28, no. 3, pp. 1356–1363, Jul. 2013.
- [17] M. Enomoto, K. Sano, J. Kanno, and J. Fukushima, "Continuous operation of wind power plants under pole-to-ground fault in an HVDC system consisting of half-bridge MMCs and disconnecting switches," *IEEE Trans. Power Electron.*, vol. 38, no. 3, pp. 3812–3823, Mar. 2023.
- [18] The Japan Electric Association, "Grid-interconnection code," JEAC 9701–2019, 2019.
- [19] D. Suzuki, N. Kawakami, M. Mori, and T. Uchiumi, "Commissioning test and operation results of new Hokkaido-Honshu HVDC link," in *Proc. Int. Power Electron. Conf.*, Himeji, Japan, 2022, pp. 2052–2056.
- [20] K. Sano and H. Nakayama, "A fault protection method for avoiding over-voltage in symmetrical monopole HVDC systems by half-bridge MMC," *IEEE Access*, vol. 9, pp. 165219–165226, 2021.
- [21] M. Li, Y. Luo, J. He, Y. Zhang, and A. P. S. Meliopoulos, "Analytical estimation of MMC short-circuit currents in the AC in-feed steady-state stage," *IEEE Trans. Power Del.*, vol. 37, no. 1, pp. 431–441, Feb. 2022.
- [22] M. Backman, L. Liljestränd, F. Rafatnia, and R. Du, "Passive DC neutral breaker for bipolar HVDC schemes," in *Proc. 4th Int. Conf. Electric Power Equip. Switching Technol.*, Xi'an, China, 2017, pp. 347–351.
- [23] J. Descloux, B. Raison, and J. -B. Curis, "Protection strategy for undersea MTDC grids," in *Proc. IEEE Grenoble Conf.*, Grenoble, France, 2013, pp. 1–6.



Mitsuyoshi Enomoto (Graduate Student Member, IEEE) received the B.S. and M.S. degrees in electrical and electronic engineering, in 2020, 2022, from Tokyo Institute of Technology, Tokyo, Japan, respectively, where he is currently working toward the Ph.D. degree in electrical and electronic engineering.

His research interests include HVDC transmission system.



Kenichiro Sano (Member, IEEE) received Ph.D. degree in electrical and electronic engineering from the Tokyo Institute of Technology, Tokyo, Japan, in 2010.

From 2008 to 2010, he served as a JSPS Research Fellow DC1. Subsequently, he was a Research Scientist with the Central Research Institute of Electric Power Industry. In 2018, he joined the Tokyo Institute of Technology, where he is currently an Assistant Professor with the Department of Electrical and Electronic Engineering. His current research interests include power electronics for power system

applications, high-voltage dc transmission systems, and power system quality.

Dr. Sano has been honored with the Outstanding Research Award from the Japan Power Academy in 2021, and the Outstanding Technical Paper Award from the Institute of Electrical Engineers of Japan in 2019 and 2007. He was an Academic Visitor with the University of Strathclyde and RWTH Aachen University, in 2023.



Junichi Fukushima received the M.S. degree in electrical and electronic engineering from Seikei University, Tokyo, Japan, in 2010.

In 2010, he joined the Tokyo Electric Power Company (TEPCO), where he was engaged in planning and operation of hydroelectric power plants and substations. He is currently the Researcher with R&D Department, TEPCO Research Institute. His research interests include power electronics, HVDC transmission system.



Junya Kanno received the M.S. and Ph.D. degrees in electrical and electronic engineering from Meiji University, Tokyo, Japan, in 1992 and 1997, respectively.

In 1992, he joined the Tokyo Electric Power Company (TEPCO), Japan, where he is currently the Senior Researcher with R&D Department, TEPCO Research Institute. His research interests include power electronics, HVDC transmission system and photovoltaic power generation.